Mon. Not. R. Astron. Soc. **000**, 1–7 (2007) Printed 17 July 2007 (MN LATEX style file v2.2)

Evolution of Massive Haloes in non-Gaussian Scenarios

M. Grossi[1,2], K. Dolag[1], E. Branchini[3], S. Matarrese[4,5], L.Moscardini[2,6]
[1] *Max-Planck Institut fuer Astrophysik, Karl-Schwarzschild Strasse 1, D-85748 Garching, Germany (margot,kdolag@mpa-garching.mpg.de)*
[2] *Dipartimento di Astronomia, Università di Bologna, via Ranzani 1, I-40127 Bologna, Italy (lauro.moscardini@unibo.it)*
[3] *Dipartimento di Fisica, Università di Roma TRE, via della Vasca Navale 84, I-00146, Roma, Italy (branchin@fis.uniroma3.it)*
[4] *Dipartimento di Fisica, Università di Padova, via Marzolo 8, I-35131, Padova, Italy (sabino.matarrese@pd.infn.it)*
[5] *INFN, Sezione di Padova, via Marzolo 8, I-35131, Padova, Italy*
[6] *INFN, Sezione di Bologna, viale Berti Pichat 6/2, I-40127 Bologna, Italy*

Accepted ???. Received ???; in original form July 2007

ABSTRACT
We have performed high-resolution cosmological N-body simulations of a *concordance* ΛCDM model to study the evolution of virialized, dark matter haloes in the presence of primordial non-Gaussianity. Following a standard procedure, departures from Gaussianity are modeled through a quadratic Gaussian term in the primordial gravitational potential, characterized by a dimensionless non-linearity strength parameter $f_{\rm NL}$. We find that the halo mass function and its redshift evolution closely follow the analytic predictions of (Matarrese et al. 2000). The existence of precise analytic predictions makes the observation of rare, massive objects at large redshift an even more attractive test to detect primordial non-Gaussian features in the large scale structure of the universe.

Key words: early universe – cosmology: theory – galaxies: clusters – large-scale of the Universe

1 INTRODUCTION

Inflation is considered the dominant paradigm for understanding the initial conditions for structure formation in the Universe. As a consequence of the assumed flatness of the inflaton potential, any intrinsic non-linear (hence non-Gaussian, NG) effect during standard single-field slow-roll inflation is generally small. Thus, adiabatic perturbations originated by the quantum fluctuations of the inflaton field during standard inflation are nearly Gaussian distributed. Despite the simplicity of the inflationary paradigm, however, the mechanism by which perturbations are generated is not yet fully established and various alternatives to the standard scenario have been considered. A key-point is that the primordial NG is model-dependent. While standard single-field models of slow-roll inflation lead to small departures from Gaussianity, non-standard scenarios for the generation of primordial perturbations in single-field or multi-field inflation allow for a larger level of non-Gaussianity (see, e.g. Bartolo et al. 2002; Bernardeau & Uzan 2002; Chen et al. 2007). Moreover, alternative scenarios for the generation of the cosmological perturbations like the curvaton (Lyth et al. 2003; Bartolo et al. 2004), the inhomogeneous reheating (Kofman 2003; Dvali et al. 2004) and the Dirac-Born-Infeld(DBI)-inflation (Alishahiha et al. 2004) scenarios, are characterized by a potentially large NG level (see for a review Bartolo et al. 2004).

Because it directly probes the primordial perturbation field, the Cosmic Microwave Background (CMB) temperature anisotropy and polarization pattern has been considered the preferential way for detecting, or constraining, primordial NG signals, thereby shedding light on the physical mechanisms for perturbation generation.

Alternatively, one can consider the Large-Scale Structure (LSS) of the Universe. This approach has both advantages and disadvantages. Unlike the CMB, which refers to a 2D dataset, LSS carries information on the 3D primordial fluctuation fields. On the other hand, the late non-linear evolution introduces NG features on its own, that need to be disentangled from the primordial ones. This can be done in two different ways: observing the high-redshift universe, such as e.g. anisotropies in the 21cm background (Pillepich et al. 2007, see also Cooray (2006)), or studying the statistics of rare events, such as massive clusters, which are sensitive to the tails of the distribution of primordial fluctuations.

So far, the investigation of the effects of NG models in the LSS has been carried out primarily by analytic means (Lucchin & Matarrese 1988; Koyama et al. 1999; Matarrese et al. 2000; Robinson et al. 2000; Robinson & Baker 2000; Verde et al. 2000, 2001; Komatsu et al. 2003; Scoccimarro et al. 2004; Amara & Refregier 2004; Ribeiro et al. 2007; Sefusatti et al. 2007; Sefusatti & Komatsu 2007; Sadeh et al. 2007). N-body simulations with NG initial conditions were performed in the early nineties (Messina et al. 1990; Moscardini et al. 1991; Weinberg & Cole 1992), but the considered NG models were rather simplistic, being based on fairly arbitrary distributions for the primordial density fluctuations (see also Mathis et al. 2004). Only very recently, Kang et al. (2007) have investigated more realistic NG models.

The suite of new N-body experiments presented in this paper

considers, for the first time, large cosmological volumes at very high-resolution for physically motivated NG models (as described in the following section). Here we focus on massive haloes and their redshift evolution. A more general and exhaustive presentation of the simulations and the main results will be done elsewhere (Grossi et al., in preparation).

This paper is organized as follows. In Section 2 we introduce the NG model here considered. The characteristics of our N-body simulations are presented in Section 3. In Section 4 we compute the halo mass function and compare it with analytic predictions. We discuss the results and conclude in Section 5.

2 NON-GAUSSIAN MODELS

For a large class of models for the generation of the initial seeds for structure formation, including standard single-field and multi-field inflation, the curvaton and the inhomogeneous reheating scenarios, the level of primordial non-Gaussianity can be modeled through a quadratic term in the Bardeen's gauge-invariant potential[1] Φ, namely

$$\Phi = \Phi_{\rm L} + f_{\rm NL}\left(\Phi_{\rm L}^2 - \langle\Phi_{\rm L}^2\rangle\right) \ , \qquad (1)$$

where $\Phi_{\rm L}$ is a Gaussian random field and the specific value of the dimensionless non-linearity parameter $f_{\rm NL}$ depends on the assumed scenario (see, e.g., Bartolo et al. 2004).

It is worth stressing that eq.(1), even though commonly used, is not generally valid: detailed second-order calculations of the evolution of perturbations from the inflationary period to the present time show that the quadratic, non-Gaussian contribution to the gravitational potential should be represented as a convolution with a kernel $f_{\rm NL}(\mathbf{x},\mathbf{y})$ rather than a product (Bartolo et al. 2005). However, for $|f_{\rm NL}| \gg 1$ as assumed in this paper, all space-dependent contributions to $f_{\rm NL}$ can be neglected and the non-linearity parameter can be effectively approximated by a constant. In this work we will take $-1000 \leqslant f_{\rm NL} \leqslant +1000$. We notice that owing to the smallness of Φ, the contribution of non-Gaussianity implied by these values of $f_{\rm NL}$ is always within the percent level of the total primordial gravitational potential, and does not appreciably affect the linear matter power spectrum.

Yet, this range is larger than that of $-54 < f_{\rm NL} < 114$, currently allowed, at the 95 per cent confidence level, by CMB data (Spergel et al. 2007). The rationale behind this choice is twofold. First of all the large scale structure provides observational constraints which are *a priori* independent of the CMB. Second of all, $f_{\rm NL}$ is not guaranteed to be scale independent, while the LSS and CMB probe different scales. Indeed some inflationary scenarios do predict large and scale-dependent $f_{\rm NL}$ (see, e.g., Chen 2005; Shandera & Tye 2006).

Departures from Gaussianity affect, among other things, the formation and evolution of dark matter haloes of mass M. One way of quantifying the effect is to look at the halo mass function which we can express as the product of the Gaussian mass function, $n_G(M,z)$, times a NG correction factor, $F_{NG}(M,z,f_{\rm NL})$:

$$n(M,z,f_{\rm NL}) = n_G(M,z)\ F_{NG}(M,z,f_{\rm NL}) \ . \qquad (2)$$

[1] on scales much smaller than the Hubble radius, Bardeen's gauge-invariant potential reduces to minus the usual peculiar gravitational potential

In the extended Press-Schecter scenario, the NG factor can be written as (Matarrese et al. 2000, hereafter MVJ)

$$F_{NG}(M,z,f_{\rm NL}) \simeq \frac{1}{6}\frac{\delta_c^2(z_c)}{\delta_*(z_c)}\frac{dS_{3,M}}{d\ln\sigma_M} + \frac{\delta_*(z_c)}{\delta_c(z_c)} \ , \qquad (3)$$

where $\delta_*(z_c) = \delta_c(z_c)\sqrt{1 - S_{3,M}\delta_c(z_c)/3}$, σ_M^2 is the mass variance at the mass scale M (linearly extrapolated to $z = 0$), and $\delta_c(z_c) = \Delta_c/D_+(z_c)$ with D_+ the growing mode of linear density fluctuations and Δ_c the linear extrapolation of the overdensity for spherical collapse. The quantity $S_{3,M}$ represents the normalized skewness of the primordial density field on scale M (linearly extrapolated to $z = 0$), namely $S_{3,M} \equiv \frac{\langle\delta_M^3\rangle}{\sigma_M^4} \propto -f_{\rm NL}$ [see, e.g., eqs.(43-45) in MVJ, in which notation $f_{\rm NL} \to -\varepsilon$ in Model B]; δ_M represents the density fluctuation smoothed on the mass scale M. The redshift dependence is only through z_c, the collapse redshift, which, in the extended Press-Schechter approach, coincides with the considered epoch, i.e. $z_c = z$.

A more robust statistics, that we will use throughout this paper, is the ratio $R_{NG}(M,z,f_{\rm NL})$ of the NG cumulative mass function $N_{\rm NG}(>M,z,f_{\rm NL})$ to the corresponding Gaussian one. Since in the high-mass tail $N(>M,z) \sim n(M,z)\times M$, we can approximate $R_{NG}(M,z,f_{\rm NL}) \simeq F_{NG}(M,z,f_{\rm NL})$ (Verde et al. 2001). We notice that, being defined as a ratio, R_{NG} is almost independent of the explicit form assumed for $n_G(M,z)$. We found, however, that the mass function in our simulation with Gaussian initial conditions is well fitted by the Sheth & Tormen (1999) relation.

An alternative approximation for R_{NG} can obtained starting from eq.(62) of MVJ: $R_{NG} \simeq P_{NG}(>\delta_c|z,M)/P_G(>\delta_c|z,M)$, where

$$P_{NG}(>\delta_c|z,M) \simeq \frac{1}{2} - \frac{1}{\pi}\int_0^\infty \frac{d\lambda}{\lambda}\exp\left(-\frac{\lambda^2\sigma_M^2}{2}\right) \times \sin\left(\lambda\delta_c + \frac{\lambda^3\langle\delta_M^3\rangle}{6}\right) \ , \qquad (4)$$

that reduces to the Gaussian case $P_G(>\delta_c|z,M)$ when $\langle\delta_M^3\rangle = 0$. As we will see, this formula provides a better fit for large positive values of $f_{\rm NL}$, while the previous one should be preferred when $f_{\rm NL}$ is large and negative.

3 NUMERICAL SIMULATIONS

We have used the GADGET-2 numerical code (Springel 2005) to perform two different sets of N-body simulations using collisionless, dark matter particles only.

The first set consists of 7 different simulations characterized by different values of $f_{\rm NL}$ but the same ΛCDM model with mass density parameter $\Omega_m = 0.3$, baryon density $\Omega_b = 0.04$, Hubble parameter $h = H_0/(100\ {\rm km\ s^{-1}\ Mpc^{-1}}) = 0.7$, primordial power law index $n = 1$ and $\sigma_8 = 0.9$, in agreement with the WMAP first-year data (Spergel et al. 2003). In all experiments we have loaded a computational box of 500^3(Mpc/h)^3 with 800^3 dark matter particles, each one with a mass of $m = 2.033\times10^{10}\ {\rm M_\odot\ h^{-1}}$. The force was computed using a softening length $\epsilon_l = 12.5\ {\rm h^{-1}}$ kpc. To set the initial conditions we have used the same initial Gaussian gravitational potential $\Phi_{\rm L}$ characterized by a power-law spectrum $P(k) \propto k^{-3}$ which was then inverse-Fourier transformed to get the NG term $f_{\rm NL}\left(\Phi_{\rm L}^2 - \langle\Phi_{\rm L}^2\rangle\right)$ in real space, and then transformed back to k-space, to account for the CDM matter transfer function. This procedure has been adapted from the original one of (Moscardini et al. 1991) and guarantees that all the $f_{\rm NL}$ models have the same linear power spectrum as the Gaussian case, as

we checked in the different realizations. The gravitational potential was then used to displace particles according to the Zel'dovich approximation, starting from a glass-like distribution. Besides the Gaussian case ($f_{\rm NL} = 0$), we have explored 6 different NG scenarios characterized by $f_{\rm NL} = \pm 100\ , \pm 500$ and $\pm\, 1000$.

The second set of simulations is designed to match those of (Kang et al. 2007). Therefore, we have used smaller boxes of 300^3(Mpc/h)^3 with 128^3 particles and a different choice of cosmological parameters ($\Omega_m = 0.233$, $\Omega_\Lambda = 0.762$, $H_0 = 73\ {\rm km\ s^{-1}\ Mpc^{-1}}$ and $\sigma_8 = 0.74$), in agreement with the WMAP three-year data (Spergel et al. 2007). We have used the same procedure to generate the primordial NG, in order to explore the cases of $f_{\rm NL} = (-58, 0, 134)$, investigated by (Kang et al. 2007).

4 THE HALO MASS FUNCTION

To extract the dark matter haloes in the simulations we have used two standard algorithms: the *friends-of-friends* and the *spherical overdensity* methods. The haloes, identified using a linking length of 0.16 times the mean interparticle distance, contain at least 32 particles.

In Fig. 1 we show the spatial positions of the dark haloes (circles) in the first set of simulations, superimposed on the mass density field (colour-coded contour plots), in a redshift slice of thickness 25.6 Mpc/h cut across the computational box. The maps are shown at four different redshifts, indicated in the plots, to follow their relative evolution (from top to bottom). The panels in the central column refer to the standard Gaussian case. The two extreme NG cases of $f_{\rm NL} = -1000$ and $f_{\rm NL} = +1000$ are illustrated in the panels in the left and right columns, respectively. The mass density fields look very similar in the Gaussian and NG cases at all redshifts. Deviations from Gaussianity become apparent only when considering, at a given epoch, the number and distribution of the top-massive, virialized objects. This is particularly evident in the $z = 2.13$ snapshot, in which the first-forming cluster-sized haloes can only be seen in the $f_{\rm NL} = +1000$ and $f_{\rm NL} = 0$ scenarios, in which cosmic structures are indeed expected to form earlier with respect to the $f_{\rm NL} = -1000$ case.

The visual impression is corroborated by the plots of Fig. 2 in which we show the cumulative halo mass function of all models in the first set of simulations, considered at the same redshifts as Fig. 1. The number density of massive objects increases with $f_{\rm NL}$, as expected, and the differences between models increases with the redshift, confirming that the occurrence of massive objects at early epochs provides an important observational test for NG models.

In Fig. 3 we show the logarithm of the ratio of the cumulative halo mass functions of NG and Gaussian models, $R_{NG}(M, z, f_{\rm NL})$, for our N-body simulations (symbols) compared to the theoretical predictions of MVJ (solid curves). Filled circles and triangles, that refer to $f_{\rm NL} = +100$ and -100, are compared to theoretical predictions of both eqs. (3) and (4) (solid and dotted lines, respectively). The agreement between model and simulation is striking. Apparent deviations are well within the Poisson errors that we do not show to avoid overcrowding. Models and simulations are still in agreement, within the errors, for $|f_{\rm NL}| = 500$ (open circles and triangles) and $|f_{\rm NL}| = 1000$ (not shown in the figure) and out to $z \sim 5$, i.e. when the validity of the MVJ approximated expressions starts breaking down: we only notice that the analytic model tends to slightly overpredict the difference between NG and Gaussian cases. In particular, we have found that eq. (4) is a better approximation to large, positive $f_{\rm NL}$, while eq. (3) is to be preferred when $f_{\rm NL}$ is negative.

This result is at variance with that of Kang et al. (2007) in which the disagreement with the MVJ predictions is already significant at the more moderate values of $f_{\rm NL} = -58$ and $f_{\rm NL} = +134$, as it is clearly illustrated in the bottom panels of their Fig. 2. To investigate whether the mismatch is genuine or is to be ascribed to numerical effects we have repeated the same analysis using the second set of simulations. We still found an excellent agreement between numerical experiments and theoretical expectations, which adds to the robustness of our results.

5 DISCUSSION AND CONCLUSIONS

The numerical experiments performed in this work show the validity of the analytic model proposed by Matarrese et al. (2000) for the halo mass function in NG scenarios. The model fits the results of our numerical experiments over a large range of $f_{\rm NL}$ and out to high redshifts despite the fact that non-Gaussianity is treated as perturbation of the underlying Gaussian model. The good match with the numerical experiments is, however, not surprising, since deviations from Gaussianity in the primordial gravitational potential are within the percent level, despite the large values used for $f_{\rm NL}$. This result is in disagreement with that of Kang et al. (2007) who found a number density of haloes larger (smaller) than ours for NG models with the same positive (negative) $f_{\rm NL}$ values. The mismatch can be ascribed neither to resolution effects nor to the background cosmology adopted in the numerical experiments and, perhaps, should be traced back to a different setup in the NG initial conditions.

Our result has two important consequences. The good news is that we can use an analytical model to provide accurate predictions for the mean halo abundance in NG scenarios spanning a range of $f_{\rm NL}$ well beyond the current WMAP constraints, without relying on time-consuming numerical experiments affected by shot noise and cosmic variance. The bad news is that deviations from the Gaussian model are more modest than in the Kang et al. (2007) experiments, which makes more difficult to spot non-Gaussianity from the analysis of the LSS. This, however, might not be a problem when considering the observational constraints that will be provided by next-generation surveys. Indeed, current hints of non-Gaussianity from large scale structures are rather weak as they are provided by the excess power in the distribution of 2dF galaxies at $z \sim 0$ (Norberg et al. 2002; Baugh et al. 2004), for which it is difficult to disentangle primordial non-Gaussianity from galaxy bias, and by the possible presence of protoclusters at $z \sim 4$, as traced by radio galaxies surrounded by Ly-α emitters and Ly-break galaxies (Miley et al. 2004), for which the measured velocity dispersion can be compared to theoretical predictions only including a realistic model for the velocity bias between galaxies and dark matter. However, the observational situation is going to improve dramatically, in many respects. Next-generation cluster surveys in X-ray, microwave and millimeter bands like the upcoming eROSITA X-ray cluster survey (Predehl et al. 2006), the South Pole Telescope survey (Ruhl et al. 2004), the Dark Energy Survey (Abbott et al. 2005) and the Atacama Cosmology Telescope survey (Kosowsky 2006) should allow us to detect clusters out to high redshift. The abundance of these objects is, however, more sensitive to the presence of a dark energy component than to that of a primordial non-Gaussianity, at least for $|f_{\rm NL}| \leqslant 100$. Indeed, as pointed out by Sefusatti et al. (2007), dark energy constraints from these surveys will not be substantially affected by primordial non-Gaussianity, as long as deviations from

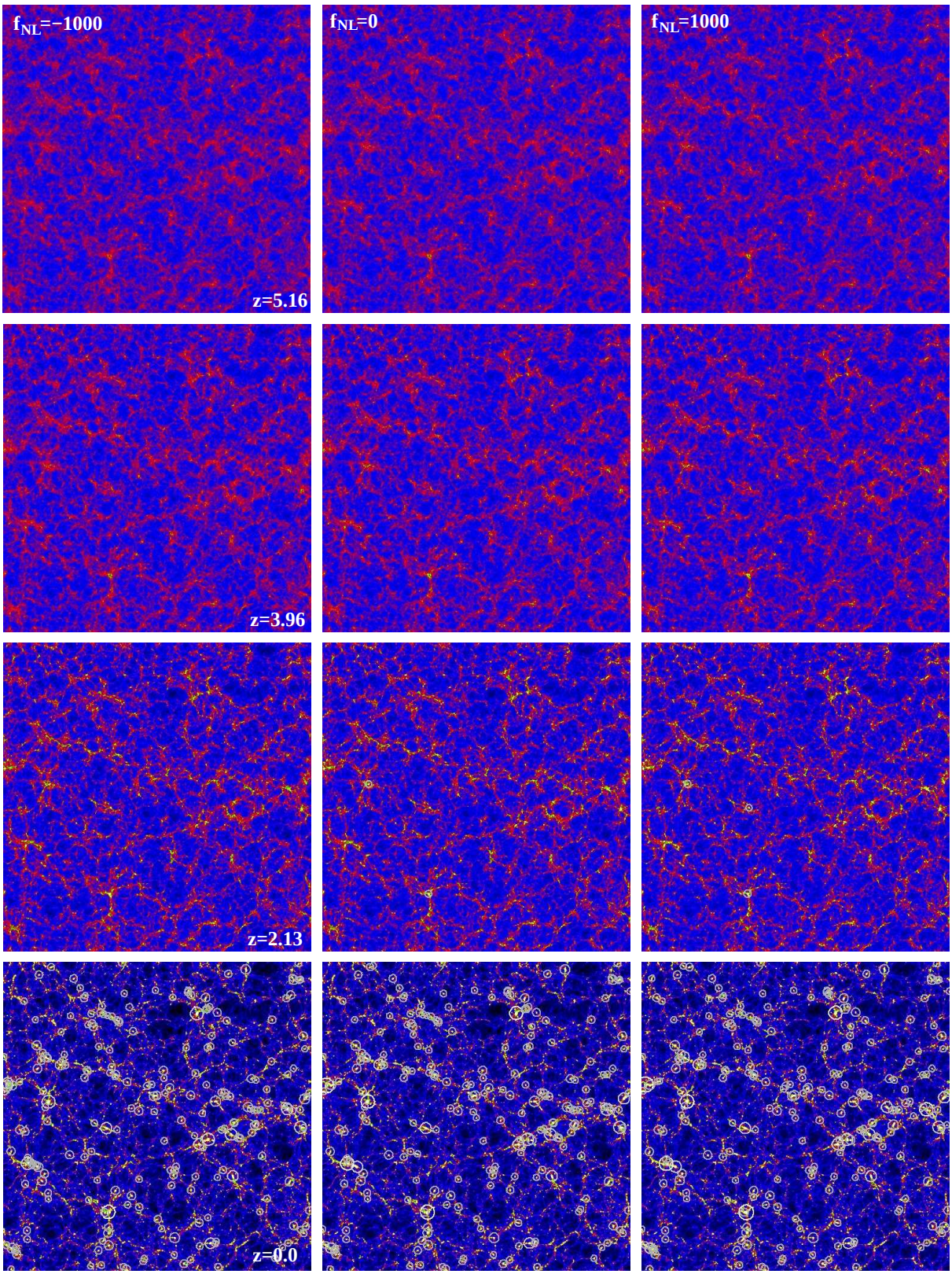

Figure 1. Mass density distribution and halo positions in a slice cut across the simulation box. The color-coded contours indicate different density levels ranging from dark (deep blue) underdense regions to bright (yellow) high density peaks. The halo positions are indicated by open circles with size proportional to their masses. Left panels: NG model with $f_{\rm NL} = -1000$. Central panels: Gaussian model. Right panels NG model with $f_{\rm NL} = +1000$. The mass and halo distributions are shown at various epochs, characterized by increasing redshifts (from bottom to top), as indicated in the panels.

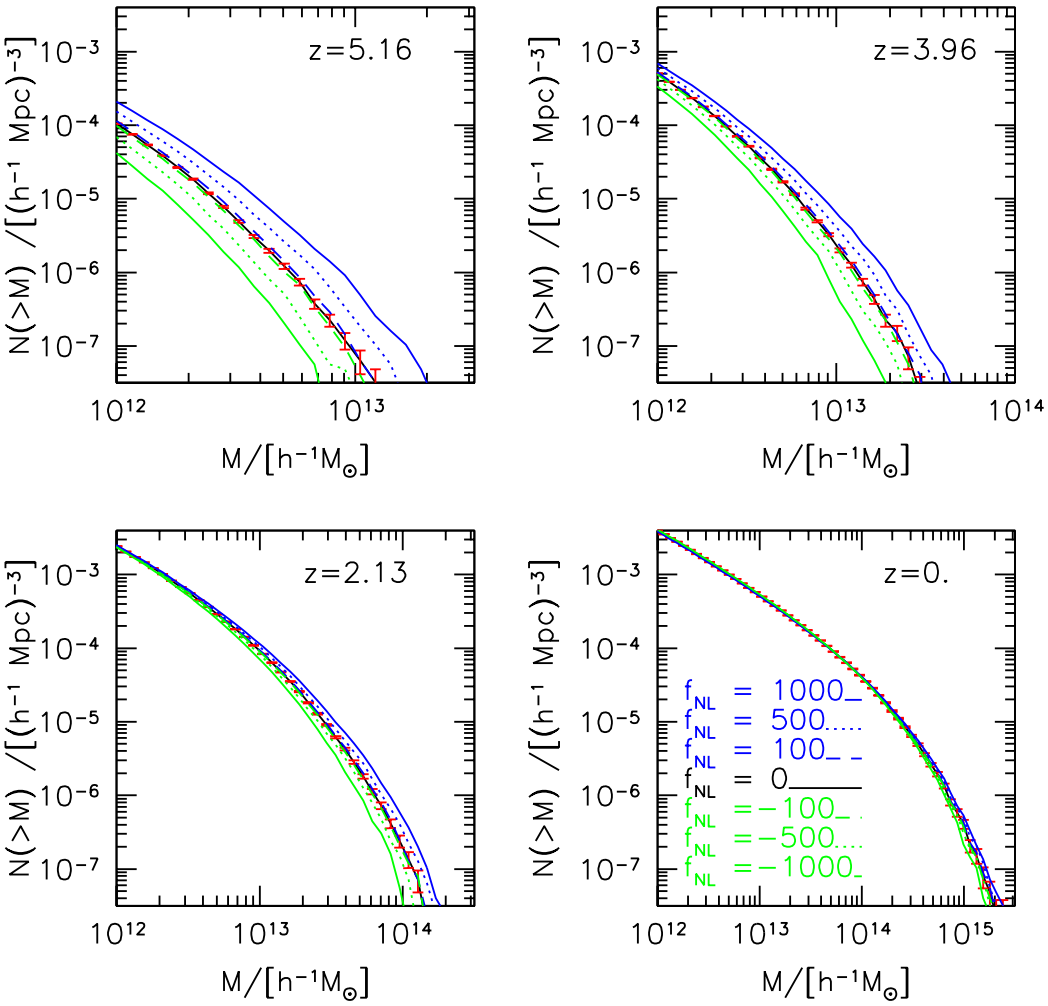

Figure 2. Cumulative mass function of the haloes in the N-body experiments at the same redshifts as in Fig. 1. The thick solid curve represents the halo mass function in the Gaussian model. Thin solid line: $f_{\rm NL} = \pm 1000$. Dotted line $f_{\rm NL} = \pm 500$. Dashed line $f_{\rm NL} = \pm 100$. The mass function of NG models with positive (negative) $f_{\rm NL}$ lies above (below) the Gaussian one. Poisson errors are shown for clarity only for the Gaussian model.

the Gaussian model do not dramatically exceed current WMAP constraints. However, these surveys could provide a fundamental cross-check on any detection of non-Gaussianity from CMB, especially from Planck since the physical scales probed by clusters differ from that of Planck by only a factor of two, allowing us to detect a possible scale dependence of non-Gaussian features. More effective constraints on both dark energy and non-Gaussianity based on statistics of rare objects is likely to be provided by the imaging of the mass distribution from gravitational lensing of high-redshift 21 cm absorption/emission signal that, if observed with a resolution of a few arcsec, will allow us to detect haloes more massive than the Milky Way back to $z \sim 10$ (Metcalf & White 2006).

Tight constraints on primordial non-Gaussianity can be set by measuring the high-order statistics of the LSS. In particular, the bispectrum analysis of the galaxy distribution at moderate z in the next-generation redshift surveys such as HETDEX (Hill et al. 2004) and WFMOS2 (Glazebrook et al. 2005) will efficiently disentangle non-linear biasing from primordial non-Gaussianity (Sefusatti & Komatsu 2007).

In this work we have demonstrated the validity of the Matarrese et al. (2000) approach to detect non-Gaussianity from the statistics of rare objects. In a future paper we will extend our analysis by considering the Probability Distribution Function of density fluctuations, that is easily obtained from our numerical simulations and that in principle can be determined by measuring the 21 cm line, either in emission or in absorption, before or after the epoch of reionization (Furlanetto 2006).

ACKNOWLEDGMENTS

Computations have been performed by using 128 processors on the IBM-SP5 at CINECA (Consorzio Interuniversitario del Nord-Est per il Calcolo Automatico), Bologna, with CPU time assigned under an INAF-CINECA grant and on the IBM-SP4 machine at the "Rechenzentrum der Max-Planck-Gesellschaft" at the Max-Planck Institut fuer Plasmaphysik with CPU time assigned to the MPA. We acknowledge financial contribution from contracts ASI-INAF I/023/05/0, ASI-INAF I/088/06/0 and INFN PD51. We thank Licia

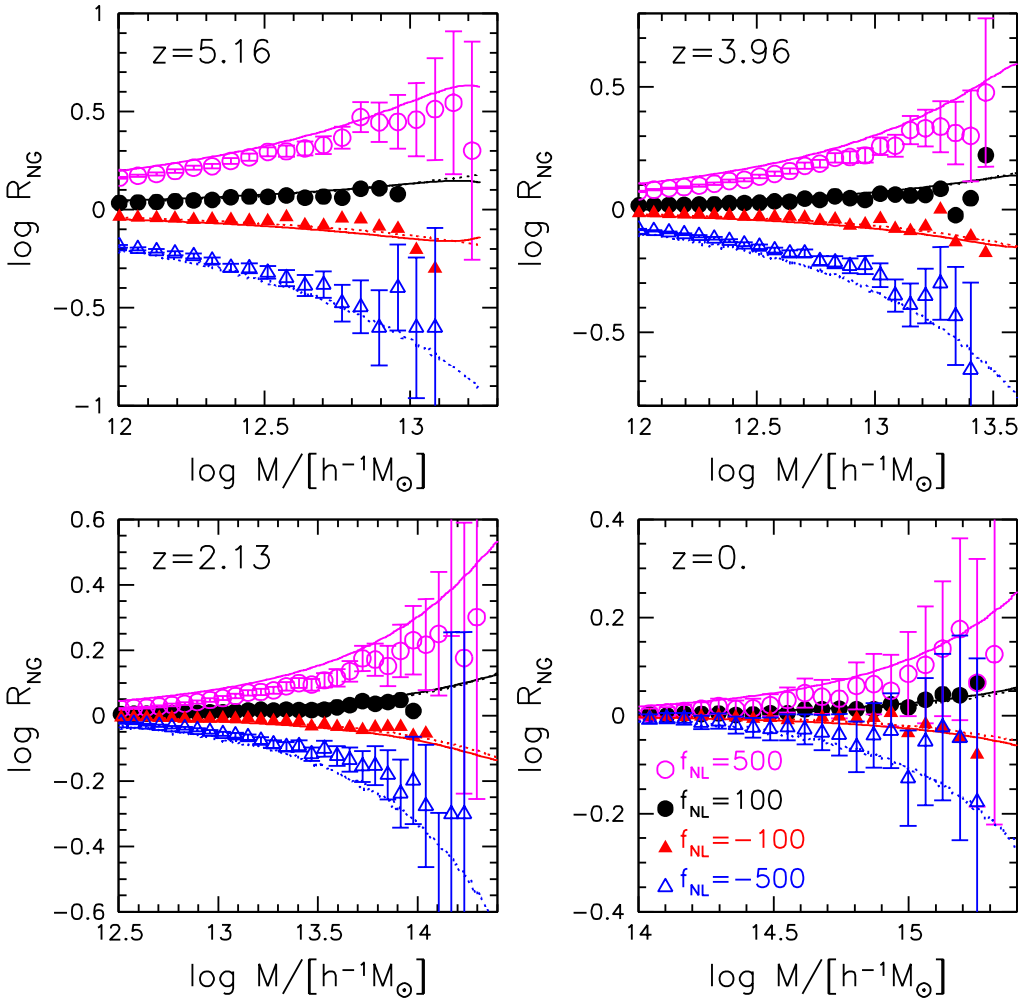

Figure 3. Logarithm of the ratio of the halo cumulative mass functions R_{NG} as a function of the mass is shown in the different panels at the same redshifts as in Fig. 1. Circles and triangles refer to positive and negative values for $f_{\rm NL}$; open and filled symbols refer to $f_{\rm NL} = \pm 500$ and $f_{\rm NL} = \pm 100$, respectively. Theoretical predictions obtained starting from eqs. (3) and (4) are shown by dotted and solid lines, respectively. Poisson errors are shown for clarity only for the cases $f_{\rm NL} = \pm 500$.

Verde for useful discussions, Shude Mao for his critical reading of the manuscript, and Claudio Gheller for his assistance.

REFERENCES

Abbott T., et al., 2005, preprint, astro-ph/0510346

Alishahiha M., Silverstein E., Tong D., 2004, Phys. Rev. D, 70, 123505

Amara A., Refregier A., 2004, MNRAS, 351, 375

Bartolo N., Komatsu E., Matarrese S., Riotto A., 2004, Phys. Rep., 402, 103

Bartolo N., Matarrese S., Riotto A., 2002, Phys. Rev. D, 65, 103505

Bartolo N., Matarrese S., Riotto A., 2004, Phys. Rev. D, 69, 043503

Bartolo N., Matarrese S., Riotto A., 2005, J. Cosmol. Astropart. Phys., 10, 10

Baugh C. M., et al., 2004, MNRAS, 351, L44

Bernardeau F., Uzan J.-P., 2002, Phys. Rev. D, 66, 103506

Chen X., 2005, Phys. Rev. D, 72, 123518

Chen X., Easther R., Lim E. A., 2007, J. Cosmol. Astropart. Phys., 6, 23

Cooray A., 2006, Phys. Rev. Lett., 97, 261301

Dvali G., Gruzinov A., Zaldarriaga M., 2004, Phys. Rev. D, 69, 023505

Furlanetto S. R., 2006, New Astron. Rev., 50, 157

Glazebrook K., et al., 2005, preprint, astro-ph/0507457

Hill G. J., Gebhardt K., Komatsu E., MacQueen P. J., 2004, in Allen R. E., Nanopoulos D. V., Pope C. N., eds, The New Cosmology: Conference on Strings and Cosmology Vol. 743 of American Institute of Physics Conference Series. pp 224–233

Kang X., Norberg P., Silk J., 2007, MNRAS, 376, 343

Kofman L., 2003, preprint, astro-ph/0303614

Komatsu E., et al., 2003, ApJS, 148, 119

Kosowsky A., 2006, New Astron. Rev., 50, 969

Koyama K., Soda J., Taruya A., 1999, MNRAS, 310, 1111

Lucchin F., Matarrese S., 1988, ApJ, 330, 535

Lyth D. H., Ungarelli C., Wands D., 2003, Phys. Rev. D, 67, 023503
Matarrese S., Verde L., Jimenez R., 2000, ApJ, 541, 10
Mathis H., Diego J. M., Silk J., 2004, MNRAS, 353, 681
Messina A., Moscardini L., Lucchin F., Matarrese S., 1990, MNRAS, 245, 244
Metcalf B. R., White S. D. M., 2006, preprint, astro-ph/0611862
Miley G. K., et al., 2004, Nat, 427, 47
Moscardini L., Matarrese S., Lucchin F., Messina A., 1991, MNRAS, 248, 424
Norberg P., et al., 2002, MNRAS, 336, 907
Pillepich A., Porciani C., Matarrese S., 2007, ApJ, 662, 1
Predehl P., et al., 2006, in Turner M. J. L., Hasinger G., eds, Space Telescopes and Instrumentation II: Ultraviolet to Gamma Ray Vol. 6266
Ribeiro A. L. B., Coelho C. M., Andrade A. P. A., Dantas M. S., 2007, A&A, 468, 19
Robinson J., Baker J. E., 2000, MNRAS, 311, 781
Robinson J., Gawiser E., Silk J., 2000, ApJ, 532, 1
Ruhl J., et al., 2004, in Bradford C. M., et al. eds, Millimeter and Submillimeter Detectors for Astronomy II Vol. 5498. pp 11–29
Sadeh S., Rephaeli Y., Silk J., 2007, preprint, astro-ph/0706.1340
Scoccimarro R., Sefusatti E., Zaldarriaga M., 2004, Phys. Rev. D, 69, 103513
Sefusatti E., Komatsu E., 2007, preprint, astro-ph/0705.0343
Sefusatti E., Vale C., Kadota K., Frieman J., 2007, ApJ, 658, 669
Shandera S. E., Tye S.-H. H., 2006, J. Cosmol. Astropart. Phys., 5, 7
Sheth R. K., Tormen G., 1999, MNRAS, 308, 119
Spergel D. N., et al., 2003, ApJS, 148, 175
Spergel D. N., et al., 2007, ApJS, 170, 377
Springel V., 2005, MNRAS, 364, 1105
Verde L., Jimenez R., Kamionkowski M., Matarrese S., 2001, MNRAS, 325, 412
Verde L., Wang L., Heavens A. F., Kamionkowski M., 2000, MNRAS, 313, 141
Weinberg D. H., Cole S., 1992, MNRAS, 259, 652